

Photochemical oxygen consumption in marine waters: A major sink for colored dissolved organic matter?

Steven S. Andrews

Chemistry Department, Stanford University, Stanford, California 94305

Sigalit Caron and Oliver C. Zafriou¹

Department of Marine Chemistry and Geochemistry, MS #4, Woods Hole Oceanographic Institution, Woods Hole, Massachusetts 02543

Abstract

Quantification of photochemical O₂ uptake provides a measure of *total* chemical photooxidation of dissolved organic matter (DOM). Here we study this process and present estimates suggesting that photooxidation has the potential to significantly modify marine DOM pools, complementing or exceeding oxidation via coupled chemical-biological pathways. We measured apparent quantum yields (AQYs) of photobleaching, O₂ uptake, and H₂O₂ production in several coastal marine samples and in dilutions of a tropical estuarine water with oligotrophic seawater. O₂-loss AQYs varied little among samples or with dilution but decreased linearly from 1.2×10^{-3} at 300 nm to 0.3×10^{-3} at 400 nm and dropped about threefold to near-constant values with increasing absorbed light dose. H₂O₂ production, about 45% of O₂ uptake, showed similar dependencies, whereas singlet oxygen (O₂(¹Δ_g)) reactions contributed less than 1% of O₂ uptake for typical coastal water. Implications of these findings for photochemical O₂, H₂O₂, and DOM cycling are discussed.

Modeling the dose-dependence of O₂ loss and photobleaching at 310 nm required three DOM pools. In the simplest case, about 90% is a weakly absorbing, low-AQY pool of DOM admixed with two similar-sized pools of more photochemically reactive DOM. This result suggests that rigorously extrapolating laboratory data to the environment requires detailed mapping of dose-wavelength-photobleaching AQY surfaces.

Action spectra and DOM flux estimates for coastal photooxidative chemistry were derived. Site-specific potential rates are comparable to available *in situ* data. Globally, the DOM photolysis capacity appears to be larger than estimated coastal DOM inputs, especially in tropical and temperate areas, including areas with maximal DOM inputs.

The major sources of oceanic dissolved organic matter (DOM) are terrestrially derived (riverine and eolian) inputs and marine-derived organic matter, *i.e.*, photosynthetically fixed carbon released by various processes. Although terrestrial DOM harbors a large biologically refractory component (Mantoura and Woodward 1983), it does not accumulate in seawater on a long timescale (Hedges *et al.* 1992), implying that nonbiological mechanisms remineralize or labilize it. Photolysis seems to provide mechanisms contributing to both roles, remineralizing some colored DOM (CDOM) to CO₂ (Miller and Zepp 1995) and labilizing some refractory DOM to metabolic attack (Kieber *et al.* 1989; Mopper *et al.* 1991; Amon and Benner 1996).

It has long been postulated that CDOM photolysis results in net oxidation of DOM (Zafriou 1977; Zika 1981), since molecular oxygen is an abundant reactive oxidant in surface waters whose photochemical activation by multiple mechanisms, such as reactions of singlet oxygen (O₂(¹Δ_g)) and of superoxide (O₂⁻) ion radical, is well known (Zafriou *et al.*

1983; Waite *et al.* 1988; Blough and Zepp 1995). Empirical evidence is also consistent with net photooxidation. For example, oxygen reduction coupled to DOM oxidation is the most plausible chemical source of H₂O₂, which exhibits rapid turnover and a large flux in surface waters (Zika 1981; Cooper *et al.* 1988; Szymczak and Waite 1988). Also, the known photoproducts of CDOM are generally more oxidized than is bulk DOM, as shown by O/C and H/C ratios. CDOM includes biogenic compounds with empirical formula CH₂O and ratios O/C = 1 and H/C = 2, as well as humic and fulvic acids with ratios O/C = 0.4–1 and H/C = 0.8–1.7 (Ikan *et al.* 1990). In contrast, photolysis produces low molecular weight carbonyl photoproducts with an empirical formula, averaged over seven products, of CH_{1.5}O (Kieber *et al.* 1990). It also produces even more highly oxidized carbon compound CO (Conrad *et al.* 1982; Valentine and Zepp 1993), carbonyl sulfide (COS; Andreae and Ferek 1992; Weiss *et al.* 1995), and especially CO₂ (Miles and Brezonik 1981; Miller and Zepp 1995).

Molecular oxygen's involvement in DOM photolysis is well known in freshwaters. Miles and Brezonik (1981) found a ratio of oxygen loss to carbon dioxide production (–O₂/CO₂) of about 2 for an iron-dependent process in “blackwaters.” Amon and Benner (1996) found up to 15% photoremineralization of DOC with a –O₂/CO₂ ratio of 1.1 in waters of the Rio Negro, a major Amazon tributary (*see* Lindell and Rai 1994; Reitner *et al.* 1997; Gao and Zepp

¹ Corresponding author.

Acknowledgments

We thank Neil V. Blough for Shark River Water samples and for numerous discussions. James W. Moffett, Bettina Voelker, Daniel J. Repeta, and reviewers provided helpful suggestions on drafts. This work was supported by NSF grants OCE-9115608 and OCE-9417214. This is contribution number 9886 from Woods Hole Oceanographic Institution.

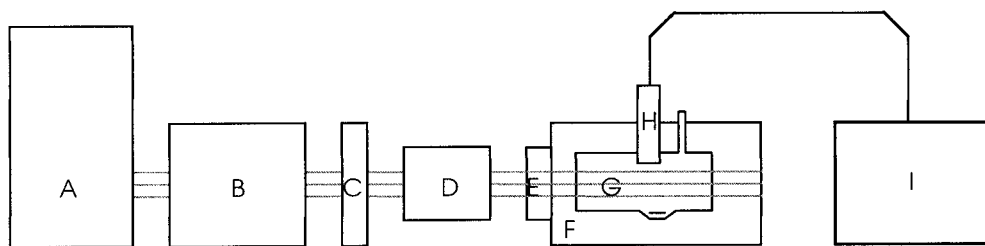


Fig. 1. Apparatus. A. 1 kW Hg-Xe lamp. B. Grating monochromator. C. Timed electronic shutter. D. Removable radiometer sensor. E. Quartz cell window. F. Water bath at 15°C; G. Sample cell and magnetic stirbar. H. Two pulsed polarographic oxygen sensors. I. Sensor controller and IBM PC as a data logger.

1998). In the only prior marine study, Laane et al. (1985) found photochemical O_2 uptake of $5 \text{ mmol m}^{-2} \text{ h}^{-1}$ in the Ems-Dollart estuary and $1.5\text{--}25 \text{ mmol m}^{-2} \text{ h}^{-1}$ in the central North Sea, equaling 5–40% of local photosynthetic O_2 production. Such high values imply significant optical, ecological, and biogeochemical roles of photooxidation in coastal environments.

There are few reported photochemical oxygen uptake measurements in less reactive waters, such as marine systems, likely due to the difficulty of measuring very small changes in oxygen concentration. Here we use sensitive, stable, pulsed dissolved O_2 probes and a drift-corrected light-minus-dark protocol to determine O_2 uptake rates and apparent quantum yields, AQYs (symbol Φ). The AQY is a unitless parameter, defined as the number of O_2 molecules that are taken up per photon absorbed by CDOM in the sample. We also determine AQY dependencies on irradiation wavelength, absorbed dose, and intensity. The relationship of oxygen loss to hydrogen peroxide formation and the role of singlet molecular O_2 reactions with DOM are examined to constrain these two major mechanistic pathways (Zafiriou et al. 1983; Blough and Zepp 1995).

Experimental protocol

Surface waters from the mouth of the Shark River (draining the Florida Everglades; salinity 14 psu), the central Gulf of Maine (salinity 30 psu), and Vineyard Sound (southeastern Massachusetts; salinity 30 psu) were filtered through $0.2\text{-}\mu\text{m}$ Nuclepore polycarbonate filters into glass or fluorinated polyethylene carboys and stored in the dark at room temperature. Oligotrophic seawaters from the Gulf of Mexico and the North Atlantic central gyre were treated similarly. Shark River water (ShRW, not to be confused with the much-studied Suwanee River Water, SRW, in related papers) diluted 1:5, 1:10, and 1:20 with oligotrophic seawater was also studied. Such mixtures are minimally perturbed, quasi-natural samples used to avoid potential artifacts associated with isolating CDOM fractions (Green and Blough 1994). CDOM absorption was measured using a Hewlett-Packard 8451a spectrophotometer referenced to Milli-Q treated distilled water (Millipore Corp.) in 5- or 10-cm pathlength cells (Blough et al. 1993). The absorption properties of ShRW have been reported previously by Green and Blough (1994). All photochemical analysis of water samples was carried out within 1 yr of the sample collection, during which time there

was no change in CDOM absorption. It was not determined whether the photoreactivity of samples changed during storage.

Irradiations, typically 1 h, were performed between 300 and 400 nm using a Spectral Energy 1-kW monochromatic illumination system with a Hg-Xe lamp (Fig. 1). The monochromator bandpass was 10 nm for irradiations up to 320 nm and 20 nm for longer wavelength irradiations to compensate for lower intensity and sample reactivity at longer wavelengths. Light intensity was measured before and after each experiment with an International Light IL1700 radiometer and calibrated for the experimental system using ferrioxalate actinometry (Hatchard and Parker 1956). Incident intensities were then converted to intensities absorbed by CDOM per unit volume ($\text{mE L}^{-1} \text{ hr}^{-1}$; $E = \text{Einsteins} = \text{moles of photons}$) for quantum yield calculations.

Dissolved oxygen was measured every 5 min by two Endeco/YSI pulsed polarographic oxygen sensors immersed in the irradiation cell out of the light path. The oxygen probes were calibrated with air-saturated water and 15% oxygen – 85% nitrogen saturated water. O_2 consumption by the sensors was shown to be negligible. Viton O-rings secured Teflon membranes on the probes and sealed them in the cell. The quartz-windowed borosilicate glass cell (8.1 cm long, 61 ml in volume) was maintained at 15°C by immersion in a temperature-controlled water bath. It was stirred magnetically and pressure-equilibrated with the atmosphere via a capillary standpipe to eliminate pressure induced sensor drift. To correct for probe drift, the electrode signal's rate of change before and after irradiations was subtracted from the average rate of loss during irradiation (Fig. 2). AQY values were computed by dividing the drift-corrected oxygen loss rate by the intensity of irradiation absorbed by CDOM. Unless otherwise indicated, AQY values were calculated using the sample's initial absorption spectrum. For long irradiations, probe drift was determined in hour-long dark periods after every 4 h of irradiation, and photobleaching was accounted for in computing apparent quantum yields.

Hydrogen peroxide, produced by 30–60-min irradiations in the same cell, was measured by a modification of the method of Miller and Kester (1988) using higher reagent concentrations (21 U ml^{-1} horseradish peroxidase (Sigma) and 1.02 mM (*p*-hydroxyphenyl)acetic acid (98%, Aldrich)) to increase the stability of the fluorescence signal, which was measured on an SLM-Aminco SPC 500C fluorometer. Hydrogen peroxide concentrations typically increased from

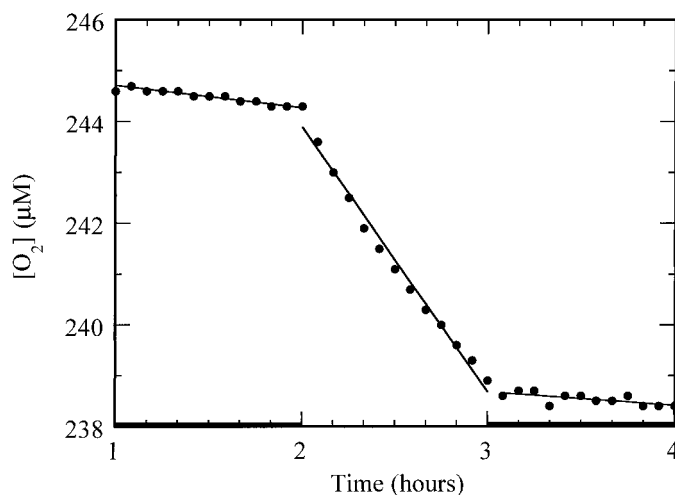


Fig. 2. Oxygen data reduction method. Points are raw data from a 310-nm irradiation of a 1:5 dilution of Shark River water at an intensity of $3.3 \text{ mE L}^{-1} \text{ hr}^{-1}$. Bars along the abscissa show dark periods before and after irradiation. Lines are least-squares fits to the data for each period. Photochemical oxygen loss rate is mean light period rate minus mean of dark period rates.

30 nM to several hundred nM during irradiation. Hydrogen peroxide production was also measured using 5–20-min irradiations in a 1-cm quartz cuvette. For these experiments, fluorometric reagents were mixed in seawater rather than with tris(hydroxymethyl)-aminomethane buffer to lower hydrogen peroxide blanks. In an attempt to directly intercalibrate the oxygen-loss and HOOH-formation methods, catalase (Sigma), which converts hydrogen peroxide quantitatively to oxygen and water, was added to some irradiated samples in the irradiation cell and the resultant oxygen increase was measured. Results were highly scattered but did not differ significantly from the measurements described above.

Singlet oxygen was produced selectively by irradiating seawater samples spiked with $1 \mu\text{M}$ Rose Bengal (RB), a singlet oxygen photosensitizer (Aldrich, 97% dye content), with 550 nm light (27 mW). From the incident light intensity, the RB photosensitization quantum yield (0.75 from Gandin et al. 1983), and the RB absorbance (86% in the cell path length), it is calculated that singlet oxygen was produced at about $1.33 \mu\text{M s}^{-1}$. The lifetime of singlet oxygen in water is about $4.4 \mu\text{s}$ (Rodgers and Snowden 1982), implying its steady-state concentration was about $5.9 \times 10^{-12} \text{ M}$. Controls showed that O_2 loss was due only to singlet oxygen reactions with DOM. Seawater irradiated with 550 nm light without RB added, exhibited photochemical oxygen uptake <3% of the uptake for the RB-sensitized sample. There was also no oxygen uptake for an irradiated solution of RB in distilled water, showing that the dye is not photo-oxidized. The light-minus-dark protocol accounted for any dark RB-DOM reactions.

Estimates of CDOM photooxidation action spectra and of regional oxygen-uptake fluxes were performed in Microsoft Excel using 24-hr daily averaged clear sky insolation spectra for different seasons (Leifer 1988), taking into account that tabulated $L(\lambda)$ values require division by 2.303 (Schwarzenbach et al. 1993, table 13.3, note c). Wavelength bin centers

and widths are: 2.5 nm (297.5–320 nm), 3.75 nm (323.3 nm), and 10 nm (330–500 nm). Insolation spectra were binned 10° latitude increments from 0° to 70°N (southern and northern hemisphere spectra were assumed identical) and combined with the latitudinal distribution of land and water in 5° bands (Sverdrup et al. 1946). Mean cloud effects were approximated by reducing clear-sky insolation by 36% (Earth's albedo). We additionally assumed that in coastal waters, CDOM absorbs all sunlight from 296.3 nm to either 445 or 505 nm, depending on whether the linear or the exponential AQY fit described below was used. This is a very good approximation up to at least 400 nm for typical coastal waters with low suspended matter and moderate pigment concentrations (Vodacek et al. 1997) and perhaps even for "blue waters" as well (Siegel and Michaels 1996). Above 400 nm, competitive absorption by plant pigments often renders the approximation inaccurate.

Oxygen AQY values were interpolated (and extrapolated beyond 400 nm) using two alternatives: a linear model and an exponential one. The "linear" fit is $\Phi(-\text{O}_2) = 0.7(3.80 \times 10^{-3} - 8.5 \times 10^{-6}\lambda)$, which is 70% of the linear fit to the oxygen data in Fig. 4. The factor of 0.7 is used to approximate overall AQYs from 1-hr AQYs shown in the figure, from the dose dependence model results (see Discussion). The linear fit clearly best captures the shape of the O_2 data. The "exponential" fit is $\Phi(-\text{O}_2) = 0.7\{8.21 \times 10^{-4}\exp[-0.018(\lambda - 340)]\}$. Again, the factor of 0.7 corrects for overall AQYs from 1-hr AQYs. The log slope of the fit is -0.012 nm^{-1} , but this is an upper limit due to dose-dependent effects, and the lower limit is -0.023 nm^{-1} . Averaging these limits gives the slope of -0.018 nm^{-1} that was used.

Results

Oxygen probe drift rates measured before and after irradiations, called dark loss rates, were used as backgrounds to be subtracted from the oxygen loss rates measured during irradiations. Pre- and postirradiation dark loss rates were similar: no systematic irradiation effect on dark loss rates was detectable although 70% of samples (not a random 50%) showed lower dark loss rates after irradiation than before. Thus, any photochemical destruction or production of dark-reactive components was either negligible or fortuitously in balance on the experimental timescale.

The AQYs of oxygen uptake (Table 1) were low enough to be difficult to measure precisely in marine samples; for this reason, our measurements did not extend above 400 nm. The robustness of the results was also increased by the "brute force" method of making many replicate runs. To separate the dependencies on various parameters with minimal complications, we intensively studied a 1:5 dilution of ShRW with oligotrophic, low-CDOM seawater, mainly at 310 nm. A dilution series (1:5, 1:10, and 1:20 ShRW) gave absorption coefficients that scaled with the dilution factor; their AQYs were all similar. While CDOM concentrations were lowered almost in proportion to the dilution factor, total (colored + uncolored) DOM concentrations probably did not change much, since the total, mostly uncolored DOM con-

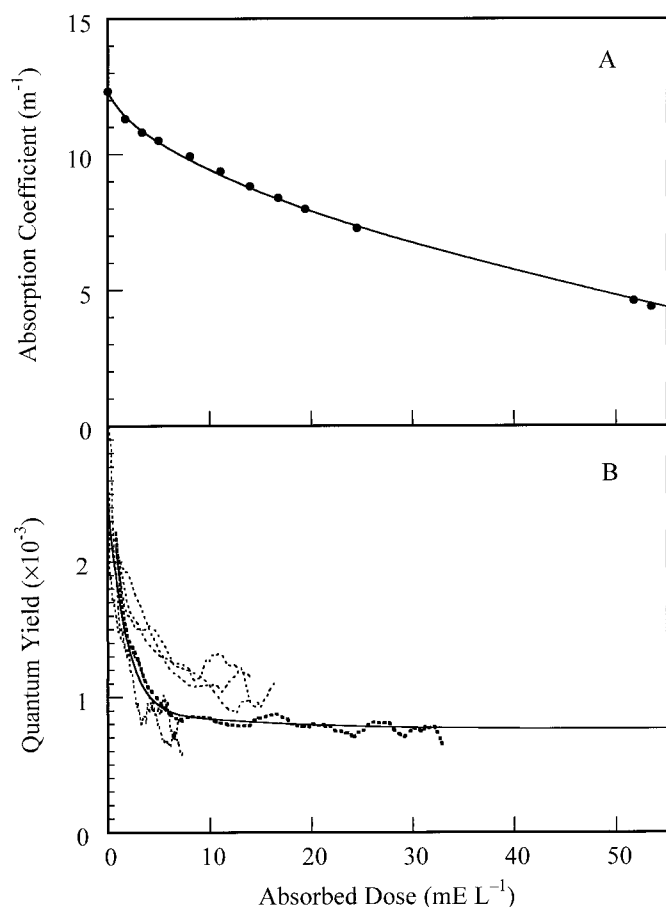


Fig. 3. Dose dependence of (A) absorbance photobleaching and (B) oxygen loss AQYs in 1:5 dilution of Shark River water in oligotrophic seawater with 310 nm irradiation. A. Points represent the 310 nm absorption coefficient. The initial absorbed intensity of 2.64 mE L⁻¹ hr⁻¹ decreased to 1.25 mE L⁻¹ hr⁻¹. B. Each jagged trace represents one run. The long run, with initial absorbed intensity 3.27 mE L⁻¹ hr⁻¹, was modeled. The smooth lines in each panel are fits by the model described (*see* text and Table 4).

concentrations of both end-member waters are likely similar. Our results thus show the behaviors expected for conservative mixing of CDOM and of the other properties that determine photoreactivity. They also imply first-order kinetics with respect to CDOM. In contrast, singlet oxygen plus CDOM reactions and radical-radical reactions would be expected to show mixed-order kinetics.

Gulf of Maine and Vineyard Sound samples also showed AQYs within 50% of those for ShRW despite their very different origins, suggesting that our results can be generalized to other riverine-influenced temperate coastal waters. In agreement with this result is the finding that very similar AQYs for fluorescence have also been measured for many different water samples (Green and Blough 1994).

Crucially, the experimental design failed to separate some variables that proved to be interdependent (in some cases, no feasible design does so). It is also difficult to compare laboratory irradiation doses to environmental doses meaningfully; for example, the former are spectrally narrow whereas the latter are broad band; lab samples were typically

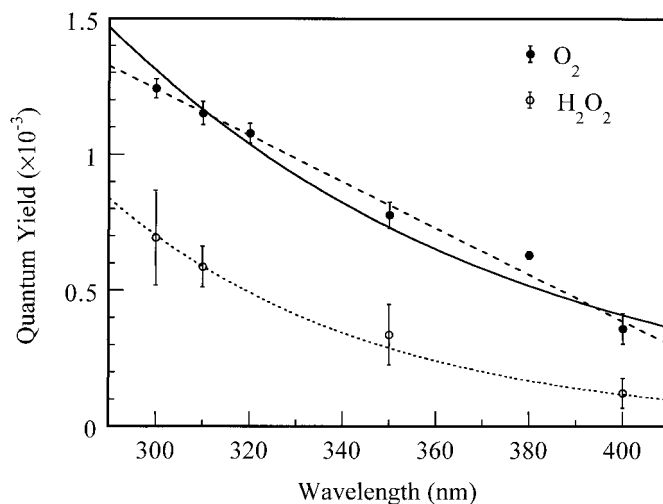


Fig. 4. Wavelength dependence of AQYs of 1:5 Shark River Water. To improve internal consistency, data shown and fit are from 1-hr irradiations with relatively large light doses. Fits shown are linear fit to oxygen data (heavy dashes) and exponential fits to both data sets. Error bars represent 1 standard deviation; points represent four to six analyses (*see* Tables 1 and 2).

more colored than most natural waters. These circumstances generate some ambiguities in interpretation, as detailed in the following paragraphs (*see* Discussion). As one example, samples' absorptions were altered by photobleaching at 310 nm, and likely at all wavelengths, during irradiation. In analyzing this effect, the most useful measure of irradiation is the absorbed light dose, which is the cumulative number of photons absorbed by CDOM. Such a comparison is presented in Table 2, and the bleaching of a sample irradiated to high doses is shown in Fig. 3A. The slope of the curve of Fig. 3A is the AQY of photobleaching at 310 nm; in this case, the AQY has units: OD/(E m⁻²). The curve is markedly nonlinear, implying that photobleaching AQYs change during the course of irradiations and that bleaching is significant and variable in the dose range of the 310 nm AQY experiments for O₂ and H₂O₂.

Based on initial sample absorbance, the AQYs for O₂ uptake ranged from about 0.4 × 10⁻³ to about 4 × 10⁻³ over the 300–400 nm region (Table 1) with relative standard deviations of about 10–20% that increased as sample transparency increased. The hydrogen peroxide data (Table 3) parallel the oxygen loss data, with about 45 ± 15% of the magnitude at a given wavelength and with slightly higher standard deviations. Both species exhibit monotonic decreases of AQYs with increasing wavelength (Fig. 4). The O₂ loss AQYs are best fit linearly with wavelength: $\Phi(-O_2) = 3.80 \times 10^{-3} - 8.5 \times 10^{-6}\lambda$ for $\lambda < 445$ nm (λ is wavelength in nm; 1 standard deviation fit errors are $\pm 7 \times 10^{-3}$ for the intercept and $\pm 2 \times 10^{-7}$ for the slope). Alternatively, both AQY data sets were fit to the more usual empirical expression analogous to that describing the absorption spectra of CDOM (Green and Blough 1994): $\Phi = Ae^{S\lambda}$ (Φ is the AQY, A is a fitted constant, and S is the slope), giving O₂ and H₂O₂ slopes of about -0.012 nm⁻¹ and -0.018 nm⁻¹, respectively. Though these slopes' statistical errors are only about 6%,

Table 1. Oxygen loss quantum yields. ShRW, Shark River water, with oligotrophic seawater dilution factor; G.M., Gulf of Maine; V.S., Vineyard Sound.

| Water source | Sample no. | Irradiation wavelength (nm) | Absorption coefficient (m^{-1}) | Absorbed intensity* ($\text{mE L}^{-1} \text{hr}^{-1}$) | Number of analyses | Average Φ ($/10^{-3}$) | Standard deviation ($/10^{-3}$) |
|--------------|------------|-----------------------------|--|---|--------------------|-------------------------------|-----------------------------------|
| 1:5 ShRW | 1 | 300 | 14.87 | 7.73 | 4 | 1.19 | 0.04 |
| 1:5 ShRW | 2 | 300 | 14.87 | 4.45 | 2 | 1.34 | 0.02 |
| 1:5 ShRW | 3 | 310 | 12.64 | 5.47 | 6 | 1.14 | 0.05 |
| 1:5 ShRW | 4 | 310 | 12.64 | 4.65 | 2 | 1.20 | 0.01 |
| 1:5 ShRW | 5 | 310 | 12.64 | 1.00 | 14 | 2.15 | 0.17 |
| 1:5 ShRW | 6 | 310 | 12.64 | 0.10 | 2 | 3.71 | 0.21 |
| 1:5 ShRW | 7 | 310 | 12.49 | 0.68 | 8 | 1.89 | 0.13 |
| 1:5 ShRW | 8 | 310 | 12.49 | 3.55 | 17 | 1.81 | 0.17 |
| 1:5 ShRW | 9 | 310 | 11.82 | 0.38 | 2 | 1.50 | 0.28 |
| 1:5 ShRW | 10 | 320 | 10.81 | 2.75 | 4 | 1.08 | 0.04 |
| 1:5 ShRW | 11 | 350 | 6.78 | 3.02 | 4 | 0.78 | 0.05 |
| 1:5 ShRW | 12 | 350 | 6.78 | 0.83 | 6 | 1.44 | 0.28 |
| 1:5 ShRW | 13 | 350 | 6.78 | 0.29 | 2 | 1.00 | 0.17 |
| 1:5 ShRW | 14 | 380 | 4.15 | 2.94 | 4 | 0.63 | 0.01 |
| 1:5 ShRW | 15 | 400 | 3.01 | 2.03 | 6 | 0.36 | 0.06 |
| 1:5 ShRW | 16 | 400 | 3.01 | 0.46 | 2 | 0.35 | 0.04 |
| 1:20 ShRW | 17 | 310 | 3.16 | 1.61 | 4 | 1.00 | 0.14 |
| 1:10 ShRW | 18 | 310 | 6.32 | 2.89 | 6 | 1.18 | 0.10 |
| ShRW | 19 | 310 | 63.19 | 7.22 | 6 | 1.81 | 0.09 |
| G.M. | 20 | 300 | 1.60 | 0.64 | 3 | 2.17 | 0.39 |
| G.M. | 21 | 310 | 0.91 | 0.08 | 4 | 2.18 | 1.28 |
| G.M. | 22 | 310 | 1.43 | 0.61 | 5 | 2.15 | 0.29 |
| G.M. | 23 | 310 | 1.27 | 0.52 | 3 | 2.05 | 0.34 |
| G.M. | 24 | 350 | 0.70 | 0.28 | 4 | 3.77 | 0.30 |
| V.S. | 25 | 310 | 1.66 | 0.67 | 3 | 1.98 | 0.19 |

* Irradiations of 1:5 ShRW were 1 hr long, so absorbed intensity equals absorbed dose (neglecting photobleaching).

the data sets are not completely comparable because of uncertainties about dose-dependent effects, explained below. Unfortunately, this uncertainty results in large effects on extrapolations of action spectra and rates to longer wavelengths, which may be important in situ.

Oxygen loss AQYs at 310 nm also proved to be strongly

dose dependent, decreasing about threefold over the course of long irradiations (Fig. 3B). The “noisy” traces in Fig. 3B were computed by dividing, at each 5-min interval, the instantaneous rate of oxygen loss (from a 30-min moving average slope of oxygen concentration) by the time-varying rate (Fig. 3A) of light absorption. Thus, Fig. 3B shows the

Table 2. Insolation comparisons for absorbed doses for 1:5 ShRW.

| Irradiation wavelength (nm) | Absorption coefficient* (m^{-1}) | Layer depth† (m) | Lab dose‡ (mE L^{-1}) | Solar intensity§ ($\text{E m}^{-2} \text{d}^{-1}$) | Bandpass sun dose (d) | Lab O_2 uptake¶ (μM) | O_2 sun dose# (d) |
|-----------------------------|---|------------------|----------------------------------|--|-------------------------|--|----------------------------|
| 300 | 15 | 0.31 | 7.7 | 0.0217 | 110 | 9.2 | 0.36 |
| 310 | 13 | 0.35 | 5.5 | 0.275 | 7.0 | 6.2 | 0.27 |
| 320 | 11 | 0.42 | 2.8 | 0.700 | 1.7 | 3.0 | 0.16 |
| 350 | 6.8 | 0.68 | 3.0 | 1.43 | 1.4 | 2.4 | 0.20 |
| 380 | 4.2 | 1.1 | 2.9 | 1.78 | 1.8 | 1.9 | 0.26 |
| 400 | 3.0 | 1.5 | 2.0 | 2.42 | 1.2 | 0.73 | 0.14 |

* For 1:5 dilution of ShRW with oligotrophic water.

† Layer depth to absorb 99% of a vertical light beam.

‡ Light dose absorbed in typical experiments (Table 1, Fig. 4).

§ Daily average clear sky solar intensity at 0° latitude, incident just below water surface, in a 10-nm bandpass centered at the appropriate wavelength (Leifer 1988).

|| Number of days of bandpassed sunlight, from the previous column, for a sample to absorb the dose of typical lab experiments.

¶ Change in oxygen concentration during a typical 1-hr lab irradiation.

Number of days of full-spectrum sunlight to achieve the same oxygen uptake as shown in the previous column. Note that a 1:50 dilution of ShRW would be more representative of typical coastal water, which raises the “sun dose” values by a factor of 10.

Table 3. Hydrogen peroxide quantum yields. ShRW, Shark River water, with oligotrophic water dilution factor.

| Water source | Sample designator | Irradiation wavelength (nm) | Absorption coefficient (m^{-1}) | Absorbed intensity ($\text{mE L}^{-1} \text{hr}^{-1}$) | Number of analyses | Average quant. yd. ($/10^{-3}$) | Standard deviation ($/10^{-3}$) |
|--------------|-------------------|-----------------------------|--|--|--------------------|-----------------------------------|-----------------------------------|
| 1:5 ShRW | A | 300 | 14.87 | 1.32–7.80 | 16 | 0.69 | 0.18 |
| 1:5 ShRW*† | B | 300 | 13.35 | 5.59 | 2 | 1.00 | 0.08 |
| 1:5 ShRW | C | 310 | 12.64 | 4.26 | 9 | 0.59 | 0.07 |
| 1:5 ShRW* | D | 350 | 6.78 | 0.84–2.90 | 15 | 0.34 | 0.11 |
| 1:5 ShRW*† | E | 350 | 6.03 | 2.35 | 2 | 0.47 | 0.02 |
| 1:5 ShRW | F | 400 | 2.60 | 1.34 | 2 | 0.17 | 0.23 |
| ShRW | G | 310 | 63.19 | 6.62 | 6 | 0.68 | 0.08 |
| ShRW* | H | 310 | 56.93 | 17.83 | 4 | 1.19 | 0.11 |
| 1:2 ShRW* | I | 310 | 28.47 | 10.16 | 3 | 1.05 | 0.14 |
| 1:10 ShRW | J | 310 | 6.32 | 2.65 | 9 | 0.69 | 0.06 |
| 1:10 ShRW* | K | 310 | 6.40 | 2.56 | 3 | 1.07 | 0.11 |
| 1:20 ShRW | L | 310 | 3.16 | 1.52 | 6 | 0.62 | 0.08 |
| 1:20 ShRW* | M | 310 | 3.19 | 1.29 | 15 | 0.82 | 0.18 |

* Analysis in 1-cm quartz cuvette, 5–20-min irradiations.

† Borate buffer (0.2 M, pH 8, 10% by volume) was added before irradiations.

best estimate of the instantaneous O_2 AQYs as a function of absorbed dose. In agreement with the figure, a $\sim 40\%$ difference in hydrogen peroxide quantum yields is seen in Table 3 between the 30–60-min irradiations and the 5–20-min irradiations.

The wavelength dependencies of AQYs for O_2 loss and for H_2O_2 formation were not measured at constant absorbed dose. Samples irradiated at >310 nm absorbed about one-third to one-half the dose of those irradiated at 310 nm due to differences in their CDOM absorption and light intensity. Thus, the wavelength dependence in Fig. 4 is flatter than it

would be if it had been measured at constant absorbed dose. Although our data do not permit a unique separation of the wavelength and absorbed dose effects, limits may be set as follows. The S values given above place upper limits (least negative values, flattest curves) on the wavelength dependence at constant absorbed dose. Assuming a maximum threefold difference between low and high dose, AQYs nearly doubles S values from -0.012 nm^{-1} and -0.018 nm^{-1} for O_2 and H_2O_2 , respectively, to lower limits of -0.023 nm^{-1} and -0.029 nm^{-1} . Thus, the wavelength dependencies for O_2 and H_2O_2 AQYs may in fact be very similar.

Another potentially significant variable affecting AQYs is the absorbed intensity. The irradiation intensity was varied by changing lamp current, and also by changing the dilution factor of the ShRW samples (in concentrated samples, the water in the front of the irradiation cell shades the water behind it, lowering the average irradiation intensity). As most irradiations were 1 hr long, those using lower lamp intensities and those using concentrated samples absorbed lower light doses (per chromophore) than those using brighter light or more transparent samples. Thus, again, any dose dependence of AQYs is convoluted with that for intensity. An attempt at separating the two effects based on a multipool model, presented in the Discussion, is shown with the intensity-dependence data in Fig. 5. The solid line, computed from the data in Fig. 3, is the modeled average AQY for 1-hr irradiations of a 1:5 dilution of ShRW, assuming no intensity dependence. One-hour average Φ values parallel the solid line, so that within the limits of this model and experimental errors, intensity effects were undetectable.

Photochemical oxygen uptake by CDOM via the singlet oxygen pathway was quantified by irradiating a 1:5 dilution of ShRW spiked with RB, a singlet oxygen photosensitizer, with 550 nm light. About 1 O_2 molecule was lost by singlet oxygen pathways per 2,500 $^1\text{O}_2$ formed, while at 366 nm (near the median wavelength of O_2 uptake and $^1\text{O}_2$ production in surface sunlight) about 1 O_2 molecule was lost per 50 $^1\text{O}_2$ formed; this was calculated using our AQY and Zepp and Baughman's (1978) $^1\text{O}_2$ quantum yield. Dividing these

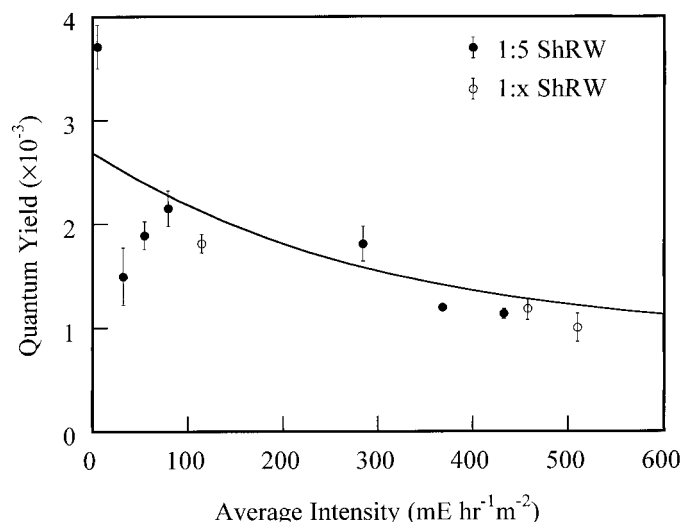


Fig. 5. Intensity dependence of AQYs. Irradiation intensity is the average intensity in the sample cell (absorbed intensity \div absorption coefficient). Solid circles represent 1:5 dilution of Shark River water; open circles are for other dilutions (from low to high intensity: no dilution, 1:10, and 1:20). Error bars represent one standard deviation; points represent 2 to 17 analyses (Tables 1, 2). The solid line was calculated from the model described, using data in figure 3 and represents the average AQY assuming no intensity dependence.

ratios shows that for this sample, about 2% of photochemical oxygen uptake is due to $^1\text{O}_2$ pathways. This estimate assumes homogeneous $^1\text{O}_2$ reaction chemistry in both CDOM- and RB-sensitized systems. If RB binds to CDOM, the true value could be even lower.

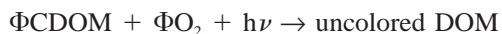
Discussion

Singlet oxygen and DOM—Singlet oxygen, although the major O_2 -derived species formed from CDOM (Blough and Zepp 1995), was not stoichiometrically significant in net O_2 consumption in the sample studied. However, singlet oxygen's AQYs are expected to lie between the first and second orders with respect to CDOM concentration, due to its consumption in parallel reactions involving water (no O_2 loss) and the DOM and CDOM pools, assuming, as is likely, that $^1\text{O}_2$ is distributed homogeneously. Thus in undiluted ShRW up to 50% of the oxygen uptake could be due to $^1\text{O}_2$ reactions, but this pathway probably accounts for <1% in more typical waters with absorption coefficients $<5\text{ m}^{-1}$ at 300 nm. However, 1% may not be negligible for some important reaction sites within DOM or CDOM pools.

Similarity of reactant and product wavelength dependencies—The wavelength-dependent trends in oxygen loss AQY data, which are fundamental to the photolysis dynamics of oxygen, parallel known AQY wavelength dependencies for several photoproducts. Monotonic decreases in AQY slopes (S values) with increasing wavelength (300–400 nm) have been reported for CO, -0.034 nm^{-1} (Kettle 1994, using data of Valentine and Zepp 1993), for H_2O_2 , -0.024 nm^{-1} (Moore et al. 1993; and our data, taking the average of the upper and lower limits; see *Results*), and for COS in blue waters -0.017 nm^{-1} (Weiss et al. 1995). Much steeper slopes are found for formation of formaldehyde, -0.065 nm^{-1} (data of Kieber et al. 1990; CDOM S value estimated from Blough et al. 1993), and for COS in Baltic samples (Zepp and Andreae 1994), -0.048 nm^{-1} .

These similar slopes suggest (but do not require) related reaction mechanisms. Similarities are expected if O_2 uptake is a consequence of reactions of the same chromophores that lead to these species, and especially if oxygen uptake is a key step in their formation mechanisms. Oxygen is a known reactant in H_2O_2 formation and is required for some CO formation processes (Redden 1982; Redden and Gordon 1982). The model results reported below suggest, however, that these qualitative parallels cannot be applied quantitatively to specific situations without further work and that the actual situation for some reactants and products is markedly more complex.

Multipool models of CDOM photochemistry—In the simplest case, seawater acts as a dilute solution of a single chromophore (or pool acting as a single substance) that is photolyzed with quantum yield Φ and reacts in a one-to-one ratio with oxygen to form transparent products:



This model predicts that the CDOM absorption decreases linearly with absorbed dose, and that the apparent oxygen

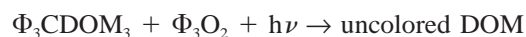
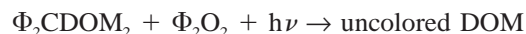
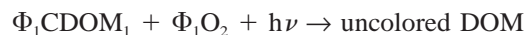
Table 4. Multipool chromophore model results.*

| CDOM pool | $[\text{CDOM}]_0$ (μM) | ϵ_{310} ($\text{M}^{-1}\text{ cm}^{-1}$) | Φ ($/10^{-3}$) |
|-----------|--|--|--------------------------|
| 1 | 76 | 520 | 0.76 |
| 2 | 4.0 | 2,600 | 1.4 |
| 3 | 3.2 | 1,000 | 26 |

* Fit for 1:5 ShRW from data in Fig. 3 and three-chromophore model described in text. $[\text{CDOM}]_0$ is the initial concentration of a model chromophore, ϵ_{310} is the decadic extinction coefficient at 310 nm, and Φ is the O_2 uptake AQY. The fit is a least-squares best fit made simultaneously to the data in Fig. 3A and to the long run in Fig. 3B with both data sets weighted equally.

uptake quantum yield (AQY) is constant over time, in contradiction to the behaviors illustrated in Fig. 3. Extending this model to include two independent chromophores, each with different quantum yields and extinction coefficients for reactions like the one above, permitted fitting either the photobleaching data or the AQY data of Fig. 3, but not both simultaneously. Fitting the AQY data required a much more reactive second chromophore than did fitting the absorption data.

Thus, modeling the dose-dependencies results requires greater complexity because both O_2 loss and photobleaching AQYs change at different rates. Although other families of models are plausible and might well also fit the data, the simple situation postulated above was extended by adding a third independent chromophore's reaction:



This model allows both data sets to be fit simultaneously, assuming a fixed ratio of oxygen uptake to CDOM loss. We define this ratio as one: CDOM concentrations are given in terms of oxygen-reactive sites. The best fit values for the parameters are shown in Table 4 for the datasets considered, 1:5 dilution of ShRW in oligotrophic seawater. The three required CDOM components are $\sim 90\%$ of a weakly absorbing, low-AQY pool of photoreactive CDOM, and a total of 10% of two similar-sized pools of more strongly absorbing and higher-AQY CDOM.

The widely varying extinction coefficients of the three CDOM pools implies that a measurement of photobleaching is not a suitable proxy for a measurement of total photooxidation. It is also seen that the AQY curve appears to approach zero slope while the absorption coefficient approaches a constant negative slope (Fig. 3). This behavior is consistent with the model's assumptions that all CDOM is photobleachable and that there are no unreactive colored products; it contradicts the possibility that a significant CDOM pool simply photosensitizes the oxidation of uncolored DOM. Extrapolating the model to zero absorption (and infinite irradiation time) indicates that the sample would be transparent after absorbing $100\text{ mE} \cdot \text{L}^{-1}$; in the process, 83 μM oxygen would be consumed. Thus the overall O_2 AQY for this sample is 8.3×10^{-4} , about 70% of a comparable

1-hr average AQY (Table 1). These results, if general, clearly indicate the need for caution in using short-term irradiations to estimate long-term geochemical rates and in assuming simple proportionality among different photoprocesses.

Photoredox budgets: Connecting C oxidation and O reduction paths—Elucidating photoredox pathways and balances remains a major challenge, since many of the steps in DOM and oxygen photoreactions occur via fast, one-electron steps, while the measurable (stable or metastable) products for both C and O species require net two-electron changes (often sums of two or four consecutive one-electron steps). For example, odd-electron O_2^- (Micinski et al. 1993) forms HOOH either by oxidizing DOM or by copper-catalyzed or DOM-catalyzed disproportionation (Zafiriou 1990; Zafiriou et al. 1998; Voelker et al. in press). Hence it is of interest to apply AQYs to characterize these electron flows (redox stoichiometries) in terms of the more plausible even-electron species of the C and O pools (e.g., $O_2 + 2e^- \rightarrow HOOH$; $O_2 + 4e^- \rightarrow HOH$). These comparisons are best done at 340 nm but are roughly wavelength-independent because O_2 and H_2O_2 show similar S values. At 340 nm, the two-electron reduction product, H_2O_2 , has an AQY of about 4×10^{-4} (Moore et al. 1993; this work), whereas the oxygen loss quantum yield (the quantum yield of oxidation of DOM by both two and four electrons per O_2) is about 9×10^{-4} . Thus, about 45% of the reaction observed is by two electrons per O_2 lost, while 55% is either by four electrons to water or by two-electron paths generating species other than HOOH, such as organic peroxides, ROOH, or ROOR. In the environment, though perhaps not in our irradiations, these organic peroxides are likely transient intermediates that yield water and more oxidized DOM, thus realizing a full four-electron DOM oxidation by O_2 . In contrast, the HOOH component of the peroxidic branch (45%) leads mainly to oxygen and water via its decomposition by biogenic catalases, partially regenerating O_2 and leaving DOM unaffected. Some HOOH enters into “peroxidase-like” DOM oxidations (Petasne and Zika 1987; Moffett and Zafiriou 1990). Thus the overall oxidation of DOM discussed above probably averages about three electrons per O_2 initially reduced.

Several components of the more complex carbon side of the photoredox budget have been studied. A likely major component of the oxidized carbon is CO_2 , with a photoproduction CO_2/CO ratio of about 20 (Miller and Zepp 1995; Gao and Zepp 1998). Taking this ratio and the CO and O_2 loss quantum yields above, the $-O_2/CO_2$ ratio is about 1.1. This ratio may be compared to reported freshwater ratios of 1.1, 1, and 2 (Amon and Benner 1996; Gao and Zepp 1998; Miles and Brezonik 1981, respectively). However, it is not feasible to budget oxidation equivalents per CO or CO_2 definitively because these products may form by oxidizing various DOM groups by paths that require varying numbers of electrons (e.g., internal redox decarboxylation, $RCHO \rightarrow RH + CO_2$ (net $0e^-$) vs. formation/decarboxylation of $RCHO_2$ radicals with subsequent O_2 uptake to form ROO radicals and thence ROOH (net $3e^-$). At 340 nm, the secondmost abundant C product, CO, has an AQY of about 4×10^{-5} (Valentine and Zepp 1993), making it a minor product in this budget. Trace products formaldehyde and other low mo-

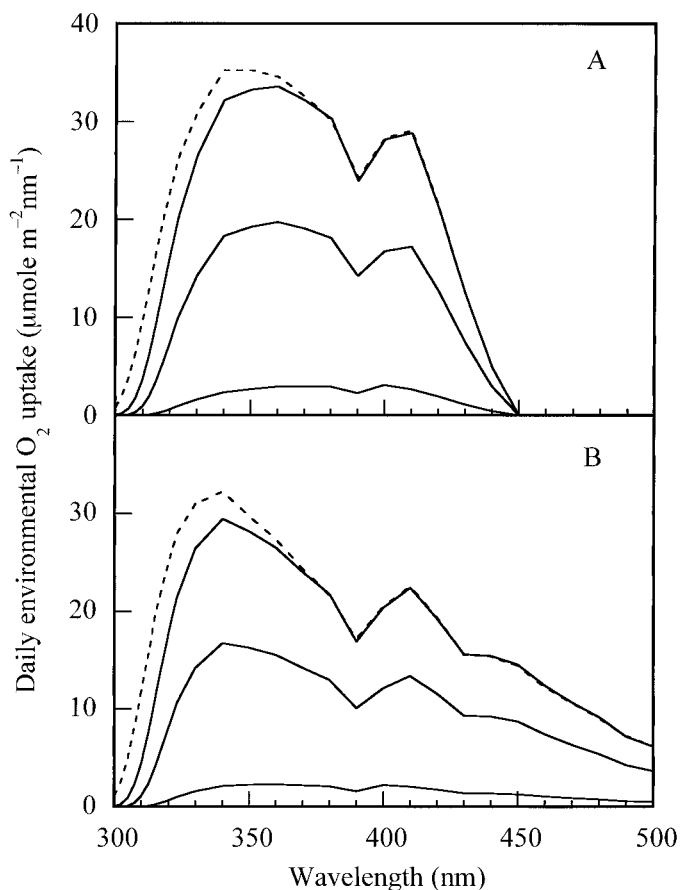


Fig. 6. Oxygen uptake action spectra for total water column photooxidation, clear sky conditions. Dashed lines are for 0° latitude (spectra are nearly identical at all seasons). Solid lines are for $70^\circ N$; in order from highest to lowest, are summer, spring, and fall spectra, and there is no midwinter insolation. A. “Linear” model. B. “Exponential” model.

lecular weight carbonyls have much larger S values than do O_2 , H_2O_2 , and CO, making comparisons less definitive; their AQYs are about equal to or less than 1×10^{-6} at 300 nm (Kieber et al. 1990). Other products, which may be significant, include those from organic peroxides and peroxy radicals, possibly forming DOM with reactive olefinic and carbonyl groups.

Action spectra and fluxes for coastal waters—Multiplying wavelength-dependent AQY data by insolation spectra results in spectral distributions of photooxidation rates (action spectra) on an area basis. This simple approach works because most ultraviolet light is absorbed by CDOM rather than water or particles in both coastal and open-ocean environments. We interpret the results in terms of coastal waters because the AQY data are derived from samples rich in coastal and terrestrial CDOM, whose contributions to blue water CDOM is currently unclear. Action spectra were calculated as a function of season and latitude for two parameterizations of the oxygen uptake data (Fig. 6) that took into account the influences of the different pools of CDOM in an approximate fashion. The wavelength-dependent oxygen

AQY data were fit with both a line, and exponential (Fig. 4); action spectra were computed for both fits. Although the linear approximation fits the data better, the exponential fit is more commonly used, and including it shows the differences between the two models. Both estimates are subject to significant uncertainties because of the following: (1) neglect of detailed multipool, dose-dependent behavior, (2) large standard deviations of the quantum yield data, (3) uncertainty regarding how accurately our samples represent typical coastal water, (4) neglect of concurrent biological DOM cycling (Kieber et al. 1989; Mopper et al. 1991), and (5) quantum yield extrapolations above 400 nm.

These action spectra show the expected relatively high photolysis rates at low latitudes and the strong seasonality at high latitudes. Because of the wide spectral range for O_2 uptake, the contribution of the ultraviolet spectrum below 320 nm (strongly affected by stratospheric ozone) is minor. Wavelengths near 350 nm are always maximally effective, but significant oxygen consumption might be due to 400–500 nm light (the extrapolated region), especially at high latitudes in the exponential-fit case. These longer wavelengths may also be especially important beneath thin river plumes overlying oligotrophic water (Sikorski and Zika 1993).

Integrating the action spectra gives estimates of environmental photochemical O_2 uptake rates. In summer at 60°N, we estimate about 3.5 mmol O_2 m^{-2} d^{-1} ; the effects of clouds and of absorption by non-CDOM chromophores may lower true rates by a factor of two (the linear and exponential models give similar results). For comparison, Laane et al. (1985) have directly measured O_2 uptake rates in spring/summer during midday in the Ems-Dollart estuary and in the central North Sea. Approximating 1 d insolation as 6 hours of clear-sky midday insolation, their data give fluxes of 5 mmol O_2 m^{-2} d^{-1} in the estuary (top 0.05 m) and in the North Sea, 1.5 mmol O_2 m^{-2} d^{-1} (top 1 m, in glass bottles), or 25 mmol O_2 m^{-2} d^{-1} (in the top 8 m in ultraviolet-transmitting bags). The flux estimated from our data and extrapolation is thus bracketed by the measurement-derived values.

Global and regional photochemical oxygen uptake fluxes—Large-scale estimates of photooxidative carbon cycling encounter further uncertainties due to the relative importance of riverine vs. coastal-derived DOM components, the ratio of DOC altered to oxygen consumed, and the photochemical importance of uncolored DOM. Regarding the first and last issues, the similar behaviors of ShRW, Vineyard Sound, and Gulf of Maine samples (Table 1) are encouraging.

The annual riverine input of DOC to the oceans is $\sim 2 \times 10^{13}$ moles C per year (Sarmiento and Sundquist 1992). There are also unknown contributions from coastal processes, including estuarine biogeochemistry, sedimentary inputs, and water-column cycling of photosynthetically derived carbon. We assume these sources are, at most, equal to riverine inputs (a flux of $\sim 2 \times 10^{13}$ moles C/yr is about 1% of coastal productivity, assuming coastal production is 25% of total marine production (Walsh 1998).

The cloud-corrected global oceanic photochemical O_2 uptake capacity (potential) was calculated from integrated action spectra to be about 3.5×10^{14} moles O_2 /yr, almost 20

times the riverine DOC input. In carbon terms, the coastal DOC-C pool can turn over in a 5-month period in coastal waters, taken as $\sim 7\%$ of the ocean's area, assuming a relatively oxygen-demanding stoichiometry of 0.5 O_2 reacting per DOC carbon altered. Such a rate is consistent with the low CDOM levels found in central gyres, since CDOM photooxidation may be faster than its horizontal transport. This plausible global result led us to make more environmentally rational turnover estimates for specific regions below.

Tropical riverine inputs may be chemically well represented by ShRW. The Amazon (15%) and Orinoco (2%), together about one-sixth of global freshwater inputs, enter the Atlantic in the northern hemisphere with maximal flows in summer and fall, providing that region with a terrestrial carbon influx per unit ocean area far higher than in other tropical regions (seasonal maxima of $\sim 2 \times 10^{12}$ mol C). These intense fluxes might be expected locally to overwhelm the photooxidation capacity, leading to a predominance of biological processing or requiring the passage of time and the spreading of plumes to process them. However, at a 0.5 : 1 O_2 : C ratio, this influx is only 2.3 times the estimated photochemical oxygen consumption in summer and in fall at 5–15°N over an area equal to that of the Caribbean basin; the eastern basin might turn over the Orinoco's inputs. These constraints are roughly consistent with field observations of the extent of the Orinoco's photochemical impact (Sikorski and Zika 1993). The Amazon plume (only partially entering the Caribbean) might likewise be processed in less than 1 yr in an area roughly the size its "retroreflection" region (Muller-Karger et al. 1988). The high O_2 photoconsumption potential in the tropics may thus be adequate to process even regionally intense inputs on subannual and subbasin scales.

Temperate regions, at least the eastern U.S. coast, may be reasonably represented by Vineyard Sound and Gulf of Maine samples (Zafriou and Dister 1991). Annual potential O_2 consumption rates are lower here than in the tropics, but riverine inputs tend to occur in spring, i.e., in and just before the season of photolysis rates approaching those in the tropics (Fig. 6, tropical vs. 70°N summer values). Thus, again it is plausible that photooxidative alteration is a major sink of these materials on regional/seasonal scales.

Latitudes above 60°N receive about 11% of the discharge of the world's largest rivers (Walsh 1998), mainly in spring and summer. The associated carbon flux, again $\sim 2 \times 10^{12}$ mol C per season, is comparable to the seasonal O_2 uptake estimates for 55°–75°N: ~ 2 – 3×10^{12} moles in spring/summer. These are likely twofold or greater overestimates due to higher cloudiness in these regions; nonetheless, at high latitudes the annual sources and photochemical sink potential seem roughly comparable. Even high-latitude materials seem potentially subject to major photoalteration in the latitudes of their origin, not necessarily requiring alternative sinks or export to sunnier climes for photolysis.

The estimates above consider photolysis in coastal waters, where it is reasonable to assume that nearly all insolation to 450 or 500 nm is absorbed by CDOM. However, the geographical distribution of photooxidizing capacity, relative to inputs, is such that large regions clearly have vast excess potential photooxidative capacity (e.g., the South Pacific). Some coastal DOM undoubtedly finds its way into blue wa-

ters where it is an “optically thin” trace constituent, which no longer absorbs all incident light. The ~90% of blue water ocean not evaluated above also seems to involve photochemical cycling of CDOM that is different from coastal CDOM. It may be formed in situ by marine processes (Siegel and Michaels 1996; Nelson et al. 1998), or be highly altered coastal DOM. Blue water DOM is not well represented by our samples, as seen by its markedly higher spectral *S* value (Blough et al. 1993; Green and Blough 1994). It also seems to cycle photochemically on seasonal timescales, perhaps involving O₂ coupled cycling analogous to the coastal CDOM photolysis discussed here.

Photochemical vs. coupled photochemical-microbial DOM cycling—It has previously been shown that coupled photochemical “priming” of CDOM, followed by microbial respiration of resultant modified DOM, is a major process for the breakdown of biologically refractory DOM (Kieber et al. 1989; Mopper et al. 1991; Amon and Benner 1996; Miller and Moran 1997). Our studies do not address the issue of the relative importance of chemical photooxidation vs. photochemical priming with subsequent biological assimilation, oxidation, or both. However, they show that photooxidative alteration deserves consideration as a sink with the potential to abiotically remineralize, or completely alter at the molecular level, geochemically significant DOM fluxes.

Summary and conclusions

Photochemical oxygen uptake, a fundamental measure encompassing many aspects of the photolysis of CDOM, has been measured directly using polarographic oxygen sensors. CDOM photolysis rates for our samples, and likely for most coastal waters, were primarily functions of irradiation wavelength and total absorbed light dose. Rates were largely independent of irradiation intensity and water source. Apparent quantum yields for O₂ loss and H₂O₂ production decreased with wavelength in the 300- to 400-nm region, with slopes similar to each other and to slopes for the dominant photo-products.

Over long irradiations, sample absorbances decreased nonlinearly with absorbed light dose, and oxygen uptake quantum yields were not constant, implying that the character of CDOM changed during irradiations. These changes were attributed to, and modeled as, multiple pools of CDOM. This finding has broad implications for a more complete understanding of coastal DOM cycling, for linking laboratory studies to fieldwork, and for modeling ocean photoprocesses. More precise measurements of these and other properties over a wider variety of conditions are needed to elucidate the generality of this finding and to characterize the functional complexity of CDOM pools.

O₂ uptake and H₂O₂ formation AQYs were used to estimate photoredox stoichiometries. The H₂O₂ production is about half that of O₂ uptake, leaving the other half to organically mediated oxygen reductions. These may include formation of organic peroxides and their decomposition products, and decarboxylation chemistry. The likely major end products of DOM oxidation are CO₂ and oxidatively altered DOM.

Photooxidation capacity for CDOM and DOM in coastal waters appears adequate to consume terrestrial DOM in its region of input at all latitudes on seasonal timescales, a result compatible with field data (Sikorski and Zika 1993; Vodacek et al. 1997). Difficult-to-study slower-reacting pools are likely subjected to much larger light doses upon mixing into blue water. Thus, understanding the factors controlling abiotic photooxidation of DOM vs. photooxidative alteration of DOM coupled to biological cycling, is clearly of major importance (Kieber et al. 1989; Mopper et al. 1991; Amon and Benner 1996).

References

- AMON, R. M. W., AND R. BENNER. 1996. Photochemical and microbial consumption of dissolved organic carbon and dissolved oxygen in the Amazon River system. *Geochim. Cosmochim. Acta* **60**: 1783–1792.
- ANDREAE, M. O., AND R. J. FERREK. 1992. Photochemical production of carbonyl sulfide in seawater and its emission to the atmosphere. *Global Biogeochem. Cycles* **6**: 175–183.
- BLOUGH, N. V., O. C. ZAFIRIOU, AND J. BONILLA. 1993. Optical absorption spectra of waters from the Orinoco River outflow: Terrestrial input of colored organic matter to the Caribbean. *J. Geophys. Res.* **98**: 2271–2278.
- , AND R. G. ZEPP. 1995. Reactive oxygen species in natural waters, p. 280–333. *In* C. S. Foote, J. S. Valentine, A. Greenberg, and J. K. Leibman [eds.], *Active oxygen: Reactive oxygen species in chemistry*. Chapman and Hall.
- CONRAD, R., W. SEILER, G. BUNSE, AND H. GIEHL. 1982. Carbon monoxide in seawater. *J. Geophys. Res. Oceans Atmos.* **87**: 8839–8852.
- COOPER, W. J., R. G. ZIKA, R. G. PETASNE, AND J. M. C. PLANE. 1988. Photochemical formation of H₂O₂ in natural waters exposed to sunlight. *Environ. Sci. Technol.* **22**: 1156–1160.
- GANDIN, E., Y. LION, AND A. VAN DE VORST. 1983. Quantum yield of singlet oxygen production by xanthene derivatives. *Photochem. Photobiol.* **37**: 271–278.
- GAO, H., AND R. G. ZEPP. 1998. Factors influencing photoreactions of dissolved organic matter in a coastal river of the Southeastern United States. *Environ. Sci. Technol.* **32**: 2940–2946.
- GREEN, S. A., AND N. V. BLOUGH. 1994. Optical absorption and fluorescence properties of chromophoric dissolved organic matter in natural waters. *Limnol. Oceanogr.* **39**: 1903–1916.
- HATCHARD, C. G., AND C. A. PARKER. 1956. A new sensitive chemical actinometer, II. Potassium ferrioxalate as a standard chemical actinometer. *Proc. Royal Soc. Lond. Ser. A* **235**: 518–536.
- HEDGES, J. I., P. G. HATCHER, J. R. ERTEL, AND K. J. MEYERS-SCHULTE. 1992. A comparison of dissolved humic substances from seawater with Amazon River counterparts by ¹³C-NMR spectrometry. *Geochim. Cosmochim. Acta* **56**: 1753–1757.
- IKAN, R., T. DORSEY, AND I. R. KAPLAN. 1990. Characterization of natural and synthetic humic substances (melanoidins) by stable carbon and nitrogen isotope measurements and elemental compositions. *Anal. Chim. Acta* **232**: 11–18.
- KETTLE, A. J. 1994. A model of the temporal and spatial distribution of carbon monoxide in the mixed layer. M.Sc. thesis, Woods Hole Oceanographic Institution/Massachusetts Institute of Technology Joint Program in Oceanography.
- KIEBER, D. J., J. MCDANIEL, AND K. MOPPER. 1989. Photochemical source of biological substrates in seawater: Implications for carbon cycling. *Nature* **341**: 637–639.
- KIEBER, R. J., X. ZHOU, AND K. MOPPER. 1990. Formation of carbonyl compounds from UV-induced photodegradation of hu-

- mic substances in natural waters: Fate of riverine carbon in the sea. *Limnol. Oceanogr.* **35**: 1503–1515.
- LAANE, R. W. P. M., W. W. C. GIESKES, G. W. KRAAY, AND A. EVERSDIJK. 1985. Oxygen consumption from natural waters by photo-oxidizing processes. *Neth. J. Sea Res.* **19**: 125–128.
- LEIFER, A. 1988. The kinetics of environmental aquatic photochemistry: Theory and practice. American Chemical Society.
- LINDELL, M. J., AND H. RAI. 1994. Photochemical oxygen consumption in humic waters. *Arch. Hydrobiol. Beih. Ergebn. Limnol.* **43**: 145–155.
- MANTOURA, R. F. C., AND E. M. S. WOODWARD. 1983. Conservative behavior of riverine dissolved organic carbon in the Severn Estuary: Chemical and geochemical implications. *Geochim. Cosmochim. Acta* **47**: 1293–1309.
- MICINSKI, E., L. A. BALL, AND O. C. ZAFIRIOU. 1993. Photochemical oxygen activation: Superoxide radical detection and production rates in the eastern Caribbean. *J. Geophys. Res.* **98**: 2299–2306.
- MILES, C. J., AND P. L. BREZONIK. 1981. Oxygen consumption in humic-colored waters by a photochemical ferrous–ferric catalytic cycle. *Environ. Sci. Technol.* **15**: 1089–1095.
- MILLER, W. L., AND D. R. KESTER. 1988. Hydrogen peroxide measurement in seawater by (*p*-hydroxyphenyl)acetic acid dimerization. *Anal. Chem.* **60**: 2711–2715.
- , AND M. A. MORAN. 1997. Interaction of photochemical and microbial processes in the degradation of refractory dissolved organic matter from a coastal marine environment. *Limnol. Oceanogr.* **42**: 1317–1324.
- , AND R. G. ZEPP. 1995. Photochemical production of dissolved inorganic carbon from terrestrial organic matter: Significance to the oceanic organic carbon cycle. *Geophys. Res. Lett.* **22**: 417–420.
- MOFFETT, J. W., AND O. C. ZAFIRIOU. 1990. An investigation of hydrogen peroxide chemistry in surface waters of Vineyard Sound with $^{18}\text{H}_2\text{O}_2$ and $^{18}\text{O}_2$. *Limnol. Oceanogr.* **35**: 1221–1229.
- MOORE, C. A., C. T. FARMER, AND R. G. ZIKA. 1993. Influence of the Orinoco River on hydrogen peroxide distribution and production in the eastern Caribbean. *J. Geophys. Res.* **98**: 2289–2298.
- MOPPER, K., X. ZHOU, R. J. KIEBER, D. J. KIEBER, R. J. SIKORSKI, AND R. D. JONES. 1991. Photochemical degradation of dissolved organic carbon and its impact on the oceanic carbon cycle. *Nature* **353**: 60–62.
- MULLER-KARGER, F. E., C. R. MCCLAIN, AND P. L. RICHARDSON. 1988. The dispersal of the Amazon's water. *Nature* **333**: 56–59.
- NELSON, N. B., D. A. SIEGEL, AND A. F. MICHAELS. 1998. Seasonal dynamics of colored dissolved organic material in the Sargasso Sea. *Deep-Sea Res. I* **45**: 931–957.
- PETASNE, R. G., AND R. G. ZIKA. 1987. Fate of superoxide in coastal sea water. *Nature* **325**: 516–518.
- REDDEN, G. D. 1982. Characteristics of photochemical production of carbon monoxide in seawater. M.S. Thesis, Oregon State Univ.
- , AND L. I. GORDON. 1982. Characteristics of the photochemical production of carbon monoxide in seawater. *Trans. Am. Geophys. Union* **63**: 990.
- REITNER, B., G. J. HERNDL, AND A. HERZIG. 1997. Role of ultraviolet-B radiation in photochemical and microbial oxygen consumption in a humic-rich shallow lake. *Limnol. Oceanogr.* **42**: 950–960.
- RODGERS, M. A. J., AND P. T. SNOWDEN. 1982. Lifetime of O_2 (Δ_g) in liquid water as determined by time-resolved infrared luminescence measurements. *J. Am. Chem. Soc.* **104**: 5541–5543.
- SARMIENTO, J. L., AND E. T. SUNDQUIST. 1992. Revised budget for the oceanic uptake of anthropogenic carbon dioxide. *Nature* **356**: 589–593.
- SCHWARZENBACH, R. P., P. M. GSCHWEND, AND D.M. IMBODEN. 1993. Environmental organic chemistry. Wiley.
- SIEGEL, D. A., AND A. F. MICHAELS. 1996. Quantification of non-algal light attenuation in the Sargasso Sea: Implications for biogeochemistry and remote sensing. *Deep-Sea Res. II* **43**: 321–345.
- SIKORSKI, R. J., AND R. G. ZIKA. 1993. Modeling mixed-layer photochemistry of H_2O_2 : Optical and chemical modeling of production. *J. Geophys. Res.* **98**: 2315–2328.
- SVERDRUP, H. U., M. W. JOHNSON, AND R. H. FLEMING. 1946. The oceans: Their physics, chemistry, and general biology, 2nd ed. Prentice-Hall.
- SZYMCZAK, R., AND T. D. WAITE. 1988. Generation and decay of hydrogen peroxide in estuarine waters. *Aust. J. Mar. Freshw. Res.* **39**: 289–299.
- VALENTINE, R. L., AND R. G. ZEPP. 1993. Formation of carbon monoxide from the photodegradation of terrestrial dissolved organic carbon in natural waters. *Environ. Sci. Technol.* **27**: 409–412.
- VODACEK, A., N. V. BLOUGH, M. D. DEGRANDPRE, E. T. PELTZER, R. K. WAITE, D. T. SAWYER, AND O. C. ZAFIRIOU. 1997. Seasonal variation of CDOM and DOC in the middle Atlantic Bight; terrestrial inputs and photooxidation. *Limnol. Oceanogr.* **42**: 674–686.
- VOELKER, B. M., D. L. SEDLAK, AND O. C. ZAFIRIOU. Chemistry of O_2^- radical in seawater: Reactions with organic Cu complexes. *Environ. Sci. Technol.* In press.
- WAITE, T. D., D. T. SAWYER, AND O. C. ZAFIRIOU. 1988. Panel I: Oceanic reactive chemical transients. *Appl. Geochem.* **3**: 9–17.
- WALSH, J. J. 1998. On the nature of continental shelves. Academic Press.
- WEISS, P. S., S. S. ANDREWS, J. E. JOHNSON, AND O. C. ZAFIRIOU. 1995. Photoproduction of carbonyl sulfide in south Pacific Ocean waters as a function of irradiation wavelength. *Geophys. Res. Lett.* **22**: 215–218.
- ZAFIRIOU, O. C. 1977. Marine organic photochemistry previewed. *Mar. Chem.* **5**: 497–522.
- . 1990. Chemistry of superoxide ion-radical (O_2^-) in seawater. *Mar. Chem.* **30**: 31–43.
- , AND B. DISTER. 1991. Photochemical free radical production rates: Gulf of Maine and Woods Hole-Miami transect. *J. Geophys. Res.* **96**: 4939–4945.
- , J. JOUSSOT-DUBIEN, R. G. ZEPP, AND R. G. ZIKA. 1983. Photochemistry of natural waters. *Env. Sci. Technol.* **18**: 358A–370A.
- , B. M. VOELKER, AND D. L. SEDLAK. 1998. Chemistry of the superoxide radical (O_2^-) in seawater: Reactions with inorganic copper complexes. *J. Phys. Chem.* **102**: 5693–5700.
- ZEPP, R. G., AND M. O. ANDREAE. 1994. Factors affecting the photochemical production of carbonyl sulfide in seawater. *Geophys. Res. Lett.* **21**: 2813–2816.
- , AND G. L. BAUGHMAN. 1978. Prediction of photochemical transformation of pollutants in the aquatic environment, p. 237–263. *In* O. Hutzinger, I. H. van Lelyveld, and B. C. J. Zoeterman [eds.], Aquatic pollutants: Transformation and biological effects. Pergamon Press.
- ZIKA, R. G. 1981. Marine organic photochemistry, p. 299–322. *In* E. K. Duursma and R. Dawson [eds.], Elsevier ocean series, v. 31. Elsevier.

Received: 11 May 1998

Accepted: 30 April 1999

Amended: 27 October 1999